

Changes in the physiology of CA1 hippocampal pyramidal neurons in preplaque CRND8 mice

Robert Wykes¹, Abigail Kalmbach, Marina Eliava², Jack Waters*

Department of Physiology, Feinberg School of Medicine, Northwestern University, Chicago, IL, USA

Received 11 January 2011; received in revised form 19 April 2011; accepted 3 May 2011

Abstract

Amyloid- β protein ($A\beta$) is thought to play a central pathogenic role in Alzheimer's disease. $A\beta$ can impair synaptic transmission, but little is known about the effects of $A\beta$ on intrinsic cellular properties. Here we compared the cellular properties of CA1 hippocampal pyramidal neurons in acute slices from preplaque transgenic (Tg+) CRND8 mice and wild-type (Tg-) littermates. CA1 pyramidal neurons from Tg+ mice had narrower action potentials with faster decays than neurons from Tg- littermates. Action potential-evoked intracellular Ca^{2+} transients in the apical dendrite were smaller in Tg+ than in Tg- neurons. Resting calcium concentration was higher in Tg+ than in Tg- neurons. The difference in action potential waveform was eliminated by low concentrations of tetraethylammonium ions and of 4-aminopyridine, implicating a fast delayed-rectifier potassium current. Consistent with this suggestion, there was a small increase in immunoreactivity for Kv3.1b in stratum radiatum in Tg+ mice. These changes in intrinsic properties may affect information flow through the hippocampus and contribute to the behavioral deficits observed in mouse models and patients with early-stage Alzheimer's disease. © 2012 Elsevier Inc. All rights reserved.

Keywords: Alzheimer's disease; Hippocampus; Pyramidal neuron; Intracellular calcium; Abeta; Beta-amyloid; Dendrite; Potassium channel

1. Introduction

The brains of patients with Alzheimer's disease (AD) contain elevated levels of β -amyloid protein ($A\beta$; Masters; et al., 1985). $A\beta$ is a peptide of 38–43 amino acids, which is liberated by sequential cleavage of amyloid precursor protein (APP). $A\beta$ peptides can be neuropathogenic and aggregate to form senile plaques, a hallmark of postmortem AD brains (Hardy, 2006). The discovery that $A\beta$ can be neurotoxic led to the amyloid hypothesis, which proposes that $A\beta$ -induced cellular dysfunction and, eventually, cell death is central to AD (Hardy and Selkoe, 2002).

An improved understanding of the effects of $A\beta$ has followed the development of transgenic mouse lines over-expressing human APP genes with mutations identified from patients with familial AD. In many of these mouse lines, $A\beta$ accumulation causes synaptic dysfunction, learning deficits, and plaque deposition. This progression mirrors AD in humans, where the early stages are often termed "mild cognitive impairment" and are characterized by subtle cognitive dysfunction in the absence of neuronal loss. Hence APP overexpressing mice are a good model in which to investigate the early effects of chronic $A\beta$ exposure in which a functional deficit, rather than a loss of neurons, underlies cognitive dysfunction.

As in AD, one of the first regions of the brain to show elevated levels of $A\beta$ in many of these mouse lines is the hippocampus, which is central to memory formation and essential for many forms of learning. Within hippocampus the principal excitatory cell type is the pyramidal neuron, and synaptic transmission between pyramidal neurons in CA3 and CA1 regions of the hippocampus has been exten-

* Corresponding author at: Northwestern University, Department of Physiology, Feinberg School of Medicine, 303 E Chicago Ave, Chicago, IL 60611, USA. Tel.: +1 312 503 0214; fax: +1 312 503 5101.

E-mail address: jackwaters@northwestern.edu (J. Waters).

¹ Current address: Department of Clinical and Experimental Epilepsy, Institute of Neurology, UCL, London, UK.

² Current address: Department of Clinical Neurobiology, German Cancer Research Center (DKFZ), Heidelberg, Germany.

sively studied in APP overexpressing mice (Palop and Mucke, 2010; Small et al., 2001). Many authors have reported deficits in long-term potentiation (LTP) and long-term depression (LTD) in the CA3–CA1 pathway in APP overexpressing mice (e.g., Brown et al., 2005; Chapman et al., 1999; Dewachter et al., 2007; Jacobsen et al., 2006; Jolas et al., 2002; Knobloch et al., 2007). LTP and long-term depression are changes in the strength of synaptic connections that are often considered to be electrophysiological correlates of learning and memory. Many of these effects occur before plaque formation (e.g., Hsia et al., 1999; Jolas et al., 2002; Larson et al., 1999). A β can also exert rapid effects on synaptic plasticity when applied to tissue from wild-type mice (Kim et al., 2001; Li et al., 2009; Nomura et al., 2005; Shankar et al., 2008; Townsend et al., 2006; Walsh et al., 2002; Wang et al., 2002, 2004; although see Raymond et al., 2003). Hence recent research has emphasized the adverse effects of A β on synapses, rather than direct effects on the intrinsic properties of neurons: their ion channels and membrane physiology.

Here we describe the changes in the intrinsic cellular function of CA1 pyramidal neurons in the CRND8 mouse model of APP overexpression. CRND8 mice carry a double human APP mutation (KM670/671NL “Swedish” and V717F “Indiana”) and overexpress APP, resulting in A β accumulation (Chishti et al., 2001). Plaque deposition first occurs at 2–3 months of age in CRND8 mice, becomes pronounced only after ~6 months of age, and plaque load increases rapidly thereafter (Chishti et al., 2001; Hyde et al., 2005; Jolas et al., 2002). CRND8 mice demonstrate cognitive impairments that initially precede plaque deposition (e.g., Ambrée et al., 2006) and progress with age. Changes in synaptic transmission also begin in CRND8 mice before plaque formation, with basal synaptic transmission being depressed at 6–9 weeks of age (Ye et al., 2010) and LTP being enhanced in both pre- and postplaque mice (Jolas et al., 2002). To identify the earliest, preplaque effects of A β , we therefore studied CA1 pyramidal neurons in acute slices from 1-week to 4-month-old CRND8 mice.

We measured a large number of intrinsic cellular parameters in CA1 hippocampal pyramidal neurons, using electrophysiological and imaging techniques and comparing the properties of young adult transgenic (Tg)⁺ mice and age-matched wild-type littermates. We found changes in intrinsic cellular properties that precede synaptic dysfunction. Our results suggest that A β affects both intrinsic cellular properties and, subsequently, synaptic dysfunction and that these effects combine to shape the network and behavioral deficits observed in CRND8 mice and perhaps in AD.

2. Methods

All experiments and procedures were approved by the Northwestern University Institutional Animal Care and Use Committee (IACUC).

2.1. CRND8 mice

A colony of CRND8 mice was established from founders provided by the University of Toronto. Mice were bred and genotyped as in previous publications (Ambrée et al., 2006; Chauhan et al., 2004; Chishti et al., 2001; Hyde et al., 2005; Jolas et al., 2002), crossing heterozygous male CRND8 mice with wild-type B6C3H females, which yields F1 mice with the transgene and wild-type littermates. The presence or absence of the transgene was determined by polymerase chain reaction (PCR) analysis of genomic DNA from tail clips, using primers for the APP Swedish (K670M/N671L) and Indiana (V717F) transgenes. All recordings were from male mice. Where possible, recordings were obtained from Tg⁺ and Tg[−] littermates and recording and analysis were performed blind to the genotype of the animal.

2.2. Acute slice preparation

Mice were deeply anesthetized with ketamine/xylazine (intraperitoneally) and transcardially perfused with cold (4 °C) modified artificial cerebrospinal fluid (ACSF) containing high sucrose and low sodium (in mM): 85 NaCl, 2.5 KCl, 1.25 NaH₂PO₄, 20 NaHCO₃, 10 4-(2-hydroxyethyl)-1-piperazineethanesulfonic acid (HEPES), 25 glucose, 75 sucrose, 0.5 CaCl₂, 4 MgCl₂, pH 7.3, oxygenated with 95% O₂/5% CO₂. The mouse was then decapitated and the brain rapidly removed into cold sucrose-ACSF. Horizontal hippocampal slices 300 μ m thick were prepared using a vibrating slicer (Vibratome, St. Louis, MO, USA) and transferred to a holding chamber containing modified ACSF at 35 °C. After 20 minutes slices were transferred to a holding chamber containing ACSF at room temperature (in mM): 125 NaCl, 2.5 KCl, 1.25 NaH₂PO₄, 20 NaHCO₃, 5 HEPES, 25 glucose, 2 CaCl₂, 1 MgCl₂, pH 7.3, oxygenated with 95% O₂/5% CO₂. Slices were used for recordings 0.5–4 hours after preparation. For recording, slices were transferred to the stage of an upright microscope (BX51W, Olympus, Center Valley, PA, USA) and constantly perfused with ACSF at 36 \pm 1 °C. Where appropriate, synaptic transmission was blocked by adding 10 μ M 2,3-dihydroxy-6-nitro-7-sulfamoyl-benzo[f]quinoxaline-2,3-dione (NBQX), 50 μ M DL-2-amino-5-phosphonopentanoic acid (AP5), and 10 μ M gabazine (6-imino-3-[4-methoxyphenyl]-1[6H]-pyridazinebutanoic acid hydrobromide) to the ACSF. After recording and imaging, slices were fixed for histological processing. Slices were fixed overnight in 4% (wt/vol) paraformaldehyde in phosphate buffer (PB; 75 mM Na₂HPO₄, 25 mM NaH₂PO₄, pH 7.4).

2.3. Electrophysiology

Somatic whole-cell recordings were obtained under visual control using infrared difference interference contrast optics (IR-DIC). Pipettes were 3–6 M Ω when filled with intracellular solution. Current-clamp recordings were obtained with an Axoclamp-2A amplifier (Molecular Devices,

Sunnyvale, CA) and the following intracellular solution (in mM): 135 K-gluconate, 4 KCl, 10 HEPES, 4 Mg-adenosine-5'-triphosphate (ATP), 0.3 Na-guanosine-5'-triphosphate (GTP), 10 Na₂-phosphocreatine, 0.2% (wt/vol) biocytin (pH 7.3, 291–293 mOsm). Voltage-clamp recordings were obtained with an Axopatch-200B amplifier (Molecular Devices) and the following intracellular solution (in mM): 110 Cs-methanesulfonate, 10 HEPES, 10 ethylene glycol-bis(2-aminoethylether)-N,N,N',N'-tetraacetic acid (EGTA), 2 Mg-ATP, 0.3 Na-GTP, 10 Na₂-phosphocreatine, 10 lidocaine N-ethyl bromide (QX-314), 5 tetraethylammonium (TEA) chloride, 5 4-aminopyridine (4-AP), 0.2% (wt/vol) biocytin (pH 7.3 with CsOH). For voltage-clamp recordings 10 μ M gabazine (SR-95531) was added to the ACSF.

Recordings were obtained from pyramidal neurons in the CA1 region of hippocampus. Pyramidal neurons were identified by the location of their somata in stratum pyramidale, by their apical dendrites (visible with infrared difference interference contrast optics and by fluorescence after obtaining a recording) and by their characteristic spiking patterns.

Excitatory postsynaptic currents (EPSCs) were evoked with a 3–5 M Ω glass pipette, filled with ACSF and placed in stratum radiatum \sim 200 μ m from the neuron. For paired-pulse stimulation, the neuron was held at -70 mV. For miniature EPSCs (mEPSCs), 1 μ M tetrodotoxin was added to the ACSF. mEPSCs were recorded for 10 minutes at a holding potential of -70 mV. In all voltage-clamp experiments series compensation (\sim 60%) was employed and recordings were discarded if series resistance was greater than 30 M Ω or changed by more than 20% during the recording.

Electrophysiological results were acquired at 20–50 kHz using National Instruments (Austin, TX) A-to-D boards and software custom-written in Labview v8.0 by J.W.

2.4. Analysis of electrophysiological results

Electrophysiological results were analyzed offline in Igor Pro v6.0 (WaveMetrics, Lake Oswego, OR, USA) using routines written by J.W. Statistical comparisons were made with GraphPad InStat v3.06, using the Mann-Whitney test unless otherwise stated.

Electrophysiological parameters were defined and measured as follows.

2.4.1. Resting input resistance

To measure resistance at the resting membrane potential, we injected 300 ms hyperpolarizing and depolarizing current steps and plot the steady-state voltage change as a function of injected current ($V - I$ relationship). The resting input resistance is the slope of the quadratic fit at 0 current (Waters and Helmchen, 2006).

2.4.2. Input resistances at -90 , -80 , -70 , and -60 mV

Slopes of the fits to the $V - I$ relationship at each membrane potential.

2.4.3. Membrane rectification

We describe rectification using the anomalous rectification coefficient (C_{AR}), derived from the quadratic fit to the $V - I$ relationship, as defined in Waters and Helmchen (2006).

2.4.4. Membrane sag

In CA1 hippocampal pyramidal neurons subthreshold currents, particularly I_h , produce a characteristic time-dependent change in membrane voltage (sag) during hyperpolarizing current injections. We measured sag with 300 ms, 500 pA hyperpolarizing current injections, defining the amount of sag as a steady state/peak voltage ratio: (steady-state $V_m - V_{rest}$)/(peak $V_m - V_{rest}$).

2.4.5. fAHP

The amplitude of the fast spike after-hyperpolarization (fAHP), defined as the difference in voltage between action potential (AP) threshold and the most hyperpolarized value within 20 ms after the downstroke of the AP crosses the threshold voltage.

2.4.6. ADP

The fAHP is often followed by an after-spike depolarization (ADP). We measured the peak amplitude of the ADP (V_m at peak $- V_{rest}$), the latency (time of peak $-$ time that AP crossed threshold) and the rate of decay of the ADP (exponential time constant of decay; exponential fit from peak of ADP).

2.4.7. Medium/slow AHP

The period of prolonged hyperpolarization after the ADP. We measured the latency (time from crossing threshold to peak), peak amplitude (relative to AP threshold), the amplitudes 1 and 3 seconds after AP threshold and 90% decay time (time from the peak of the after-hyperpolarization [AHP] to the voltage corresponding to $V_{rest} - 10\%$ of the amplitude of the medium/slow AHP).

2.4.8. Rheobase

Minimum current required to evoke 1 or more APs during a 300-ms depolarizing current step.

2.4.9. Current threshold for 10 APs

The minimum current required to evoke ten APs during a 300-ms depolarizing current step.

2.4.10. AP threshold

Voltage at which the first temporal derivative of the membrane potential exceeded 40 V per second.

2.4.11. AP amplitude

Peak voltage $-$ threshold voltage.

2.4.12. AP half width

Width of AP at half-height.

2.4.13. AP rise time

Time to rise from 10% to 90% of AP amplitude.

2.4.14. AP decay time

Time to decay from 90% to 10% of AP amplitude.

2.4.15. Paired-pulse ratio

Ratio of peak amplitudes of 2 EPSCs (amplitude of second EPSC/amplitude of first EPSC). Mean paired-pulse ratios were calculated in each neuron from at least 20 trials at each interpulse interval.

2.4.16. AMPA/NMDA ratio

Ratio of the peak EPSC amplitude at holding potentials of -70 mV to the EPSC amplitude 60 ms poststimulus at $+40$ mV. The mean (AMPA/NMDA) ratio was calculated for each neuron from EPSCs evoked alternatively at -70 and $+40$ mV for 20–50 trials.

2.4.17. mEPSC analysis

mEPSCs were detected using a routine written in Igor Pro by J.W., based on the template-matching approach of Clements and Bekkers (1997). A biexponential template with a rise time constant of 1.5–2.5 ms and a decay time constant of 6–12 ms was employed, determined for each neuron by fitting the mean of ~ 20 manually-selected EPSCs. We employed a detection threshold of -4 . We calculated the mEPSC frequency and median amplitude from a minimum of 10 minutes of continuous recording.

2.5. Calcium imaging

Intracellular calcium measurements were made using a 2-photon microscope built by J.W. on an Olympus BX51 frame. The specimen was illuminated with 840 nm light from a Ti: sapphire laser (Chameleon Ultra, Coherent (Santa Clara, CA, USA), 80 MHz repetition rate; 100–150 femto-second pulse width). Excitation light was focused onto the specimen using a $40\times$, NA 0.8 water-immersion objective (Olympus). Emitted light was collected in the epifluorescence configuration through a 680 nm dichroic reflector and an infrared-blocking emission filter (ET700sp-2p, Chroma Technology) and split into red and green channels using a second dichroic mirror (T580lpxr, Chroma Technology, Bellows Falls, VT, USA). Emission filters were a 490–560 bandpass filter and a 590–650 bandpass filter (Chroma Technology). Fluorescence was detected using photomultiplier tubes (R6357, Hamamatsu, Bridgewater, NJ). Scanning and image acquisition was controlled using custom software written in Labview by J.W.

Neurons were filled via the recording pipette with the high-affinity calcium indicator Oregon green BAPTA 488–1 (OGB-1; 100 μM) and the calcium-insensitive indicator Alexa 594 (both indicators from Invitrogen, Carlsbad, CA, USA) (10 μM). Imaging data were collected only after the amplitude of the calcium signal was constant during repeated trials, indicating that the dyes had reached steady-state concentrations (>40 minutes after breaking whole-cell). Calcium transients were monitored with 500 Hz line scans through the apical dendrite and the location of each line scan (relative to the soma) was determined with a calibrated x-y stage. Image analysis was

performed using routines written by J.W. in Igor Pro (WaveMetrics). The fluorescence of each indicator was averaged over the width of the dendrite and background (from a region of the line not containing any stained structure) was subtracted.

Intracellular calcium concentration was expressed as a G/R ratio: fluorescence ratio of OGB-1 (green indicator) and Alexa 594 (both indicators from Invitrogen) (red indicator; Oertner et al., 2002; Sabatini et al., 2002). This approach has several advantages over other methods of quantifying calcium concentration, principally that any change in the resting intracellular calcium concentration is readily apparent as a change in the resting G/R ratio. In addition, a change in intracellular calcium concentration will not directly affect measurement of the AP-evoked calcium transient.

2.6. Thioflavin staining and 6E10 immunohistochemistry

Mice were transcardially perfused with ~ 30 mL of 0.1 M phosphate-buffered saline (PBS) at pH 7.3 containing 0.7% (wt/vol) heparin, followed by 30 mL of 4% (wt/vol) paraformaldehyde in PBS (PFA). Brains were removed and stored overnight in 4% PFA at 4°C . Coronal sections (75 μm) were cut on a vibratome and washed 3 times in PBS. For Thioflavin-S (Sigma, St. Louis, MO, USA) staining, sections were incubated overnight in 1 $\mu\text{g}/\text{mL}$ Thioflavin-S and washed before mounting. For 6E10 immunohistochemistry, washed sections were placed in 1% vol/vol Triton TX-100 (in PBS) for 45 minutes, then 1% (wt/vol) bovine serum albumin (BSA) and 1% Triton TX-100 (in PBS) for 45 minutes and incubated overnight in 6E10 antibody (1:400). 6E10 immunofluorescence was visualized with a goat anti-mouse fluorescein isothiocyanate (FITC) secondary antibody. Thioflavin and 6E10-stained sections were mounted in mowiol 4-88 (Sigma) and fluorescence images were acquired by widefield microscopy.

To quantify Thioflavin-S staining, images were thresholded at twice the median intensity to create discrete fluorescent puncta. The number of puncta and summed surface area of puncta were calculated in ImageJ (rsb.info.nih.gov/ij).

2.7. Channel immunohistochemistry

Mice were transcardially perfused as described above. Brains were placed in PFA at 4°C for 1–2 hours, transferred to 10% (wt/vol) sucrose in PBS (pH 7.35) for 1 hour and allowed to sink in 30% sucrose in PBS (pH 7.35). Coronal sections (50- μm thick) were cut on a freezing microtome. Sections were rinsed 3 times in PBS, placed in 1% Triton TX-100 and 1% BSA in PBS for 1–2 hours and incubated overnight in primary antibody in 1% Triton TX-100 and 1% BSA in PBS. Antibodies were obtained from the University of California, Davis/NIH NeuroMab Facility. After 3 rinses in PBS, sections were incubated for 2 hours in rabbit anti-mouse secondary antibodies conjugated to Alexa 594 (Invitrogen), rinsed and mounted in mowiol (Sigma). Fluorescence images were acquired by widefield microscopy.

The relative intensities of fluorescence staining in stratum pyramidale, stratum radiatum, and stratum oriens were expressed as a “fluorescence distribution ratio”. For each section a region of interest was defined that included stratum pyramidale in CA1. The intensity in this region was measured, as were the intensities in two neighboring regions of identical size and shape in stratum radiatum and stratum oriens. From these raw intensities we subtracted background fluorescence, measured from sections processed with no primary antibody. We then divided the background-subtracted intensity in stratum pyramidale by the mean of the background-subtracted intensities of stratum radiatum

and stratum oriens to yield the fluorescence distribution ratio. For each mouse, intensities and distribution ratios were measured for 3–6 sections and averaged.

3. Results

3.1. Time course of APP expression and plaque deposition in CRND8 mice

Our aim was to determine the earliest changes in CA1 pyramidal neurons in CRND8 mice. Therefore we first determined the time course of APP expression and plaque

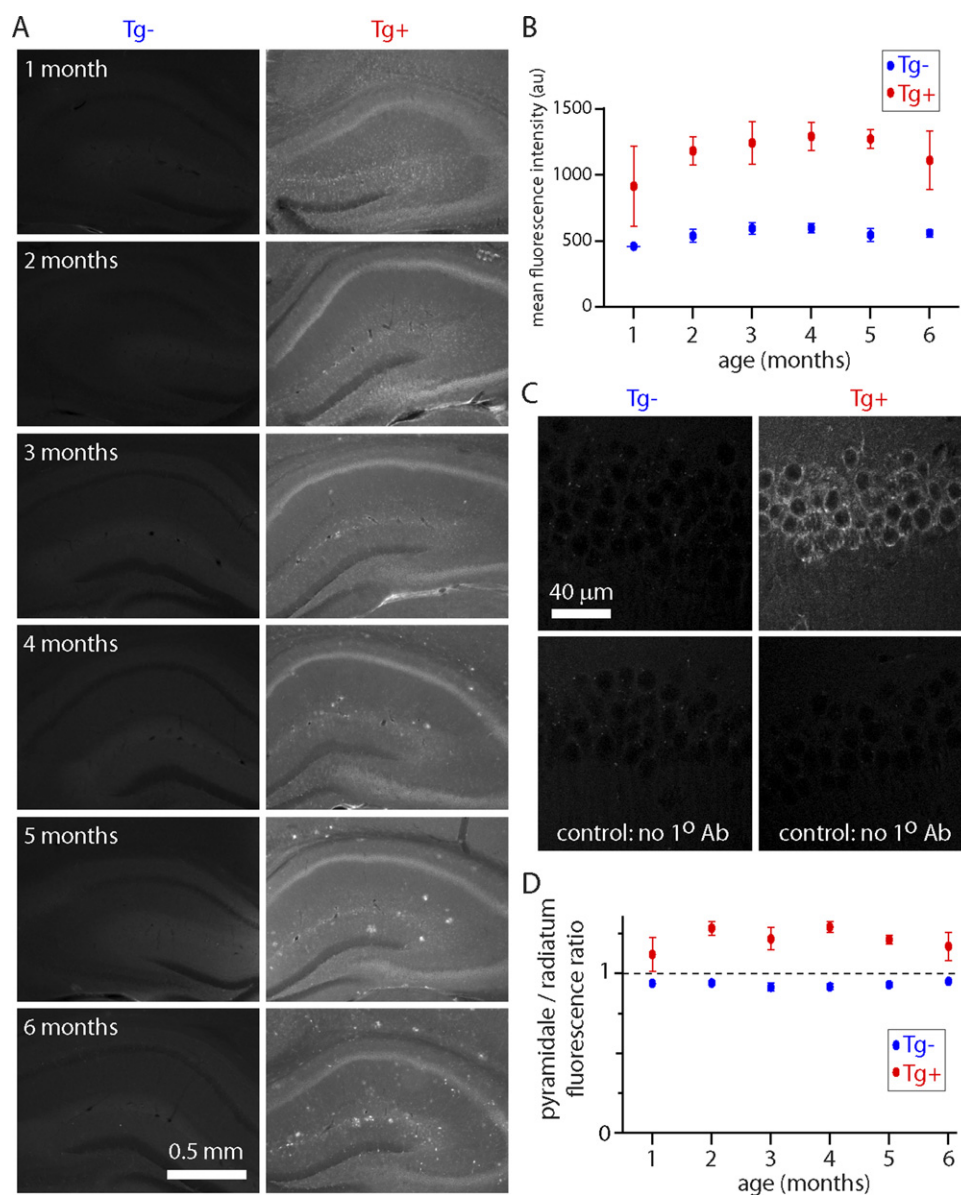


Fig. 1. 6E10 immunohistochemistry in CRND8 mice up to 6 months of age. (A) Example widefield images of 6E10 immunohistochemistry in hippocampi from transgenic (Tg+) and Tg− mice up to 6 months of age. Fixed sections 75 μ m thick. (B) Hippocampal fluorescence (mean intensity of the entire image) as a function of age. Each data point is the mean \pm standard error of the mean (SEM) of 3 regions per section from 12 sections from 2 mice. (C) Two-photon images of stratum pyramidale in Tg+ and Tg− mice at 2 months of age, including control sections to which no primary (6E10) antibody was applied. (D) Ratio of fluorescence intensity in stratum pyramidale to that in stratum radiatum. Each data point is the mean \pm SEM of 3 regions per section from 12 sections from 2 mice.

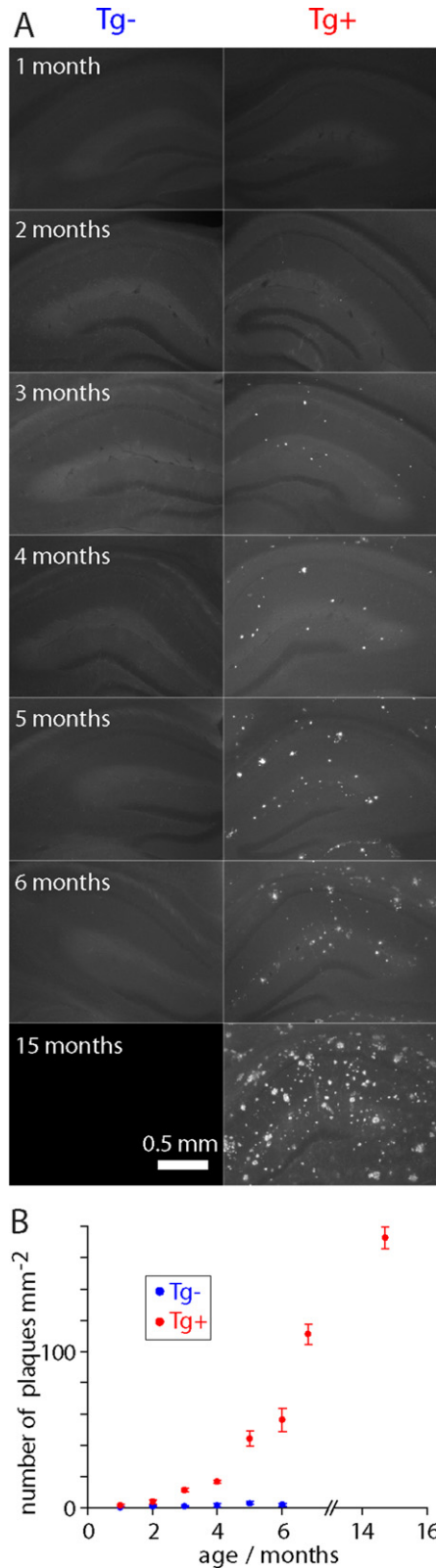


Fig. 2. Plaque load quantified with thioflavin fluorescence. (A) Example widefield images of thioflavin staining showing hippocampi from transgenic (Tg⁻) and age-matched Tg⁺ CRND8 mice up to 15 months of age. Fixed sections 75 μ m thick. (B) Plaque load as a function of age. Each data point is the mean \pm standard error of the mean (SEM) of 4 sections from 2 mice.

formation in CRND8 mice. A β expression in CRND8 mice was detected using a monoclonal 6E10 antibody, which binds to human APP and to residues 1–16 of A β , including oligomeric and deposited forms of A β (Kim et al., 1988, 1990). Mean fluorescence in hippocampus was greater in Tg⁺ than in Tg⁻ mice at all ages examined and increased with age (1–6 months; Fig. 1A and B). In Tg⁺ mice, fluorescence was particularly intense in stratum pyramidale, where 6E10 appeared to stain the cytoplasm in pyramidal neurons (Fig. 1A–D). To visualize plaques we used Thioflavin-S, which binds to amyloid fibrils but not monomers and gives a distinct spectral shift upon binding (Guntern et al., 1992; LeVine, 1999). Thioflavin-S fluorescence was negligible before 2–3 months of age and increased rapidly after 4–5 months of age (Fig. 2, Supplementary Fig. s1), consistent with previous reports (Chishti et al., 2001; Hyde et al., 2005; Jolas et al., 2002). We therefore focused our subsequent experiments on mice at 1–2 months of age, at which age APP is expressed in CRND8 mice, but there are no plaques.

3.2. Action potential waveform is narrower in Tg⁺ CRND8 mice from 1 month of age

We obtained whole-cell recordings from CA1 hippocampal pyramidal neurons in acute slices. We measured a large number of electrophysiological parameters, which together reflect the overall health of CA1 pyramidal neurons, comparing neurons in slices from CRND8 mice and wild-type littermates. By examining neurons in young animals, we aimed to identify which physiological parameters were the first to be affected in CRND8 mice.

Subthreshold parameters (such as resting membrane potential and input resistance) were similar in neurons from Tg⁺ and Tg⁻ mice at 2 months of age (no significant differences in any parameters; Table 1). However, APs were narrower in neurons from Tg⁺ than from Tg⁻ mice: AP halfwidth and decay time were both \sim 10% shorter in Tg⁺ mice (Fig. 3). The spiking pattern, voltage threshold, AP amplitude, and rise time were similar in Tg⁺ and Tg⁻ mice (Fig. 3), suggesting that the difference in AP waveform is attributable to a change in 1 or more of the currents underlying membrane potential repolarization.

Postspike potentials were unaffected (Table 1) and the difference in AP waveform was preserved during a train of 10 APs. The difference in AP waveform was also observed in 1-month-old mice, but not in 1-week-old mice (Fig. 3, Supplementary Table s1 and s2, supplementary Fig. S2), indicating that this effect developed between 1 week and 1 month of age. Hence in CA1 pyramidal neurons from CRND8 mice there is a selective narrowing of the AP waveform before changes in other electrophysiological parameters and several weeks or perhaps months before the first plaques form.

Table 1
Electrophysiological characteristics of CA1 pyramidal neurons from 2-month-old CRND8 mice

	Tg ⁻	Tg ⁺
Resting membrane potential (mV)	-63.8 ± 0.4 (n=59)	-64.4 ± 0.4 (n=49)
Resting input resistance (MΩ)	124.8 ± 3.7 (n=59)	119.4 ± 3.0 (n=49)
Input resistance at -90 mV (MΩ)	92.4 ± 3.8 (n=59)	84.1 ± 2.9 (n=49)
Input resistance at -80 mV (MΩ)	103.9 ± 3.7 (n=59)	97.0 ± 3.0 (n=49)
Input resistance at -70 mV (MΩ)	120.0 ± 3.7 (n=59)	115.7 ± 3.3 (n=49)
Input resistance at -60 mV (MΩ)	143.1 ± 5.5 (n=48)	146.1 ± 5.8 (n=44)
Anomalous rectification (MΩ/nA)	64.3 ± 4.1 (n=58)	68.1 ± 3.8 (n=49)
Sag (steady state/peak ratio)	0.85 ± 0.007 (n=33)	0.84 ± 0.006 (n=35)
Rheobase (pA)	81.8 ± 4.9 (n=59)	82.4 ± 4.8 (n=49)
Current threshold for 10 APs (pA)	180.5 ± 8.7 (n=59)	168.2 ± 6.9 (n=49)
fAHP amplitude (mV)	7.3 ± 0.92 (n=59)	5.7 ± 1.1 (n=48)
ADP amplitude (mV)	11.8 ± 0.66 (n=21)	11.4 ± 0.65 (n=20)
ADP latency (ms)	2.8 ± 0.1 (n=21)	3.0 ± 0.1 (n=20)
ADP decay time (ms)	19.8 ± 1.3 (n=21)	16.6 ± 0.9 (n=20)
Body weight (g)	28.3 ± 0.8 (n=20)	24.7 ± 0.8 (n=19)

There was no significant difference in any of the above parameters (Mann-Whitney test, $p > 0.05$), except for body weight, which was significantly smaller for transgenic (Tg⁺) than for Tg⁻ mice ($p = 0.006$).

Key: ADP, after-spike depolarization; APs, action potentials; fAHP, fast spike after-hyperpolarization; TG, transgenic.

3.3. Intracellular calcium signaling in 2 month-old CRND8 mice

It is now widely accepted that A β causes dysfunction of synaptic transmission and particularly in synaptic plasticity (Small et al., 2001). Propagation of APs into the dendritic tree and the resulting wave of calcium influx are essential in the induction of some forms of synaptic plasticity (Waters et al., 2008). A narrower AP would be expected to propagate a shorter distance into the dendritic tree and evoke less calcium influx and might therefore contribute to the deficit in synaptic plasticity in CRND8 mice.

We therefore measured AP-evoked intracellular calcium signals in CA1 pyramidal neurons, filling neurons with a calcium indicator (100 μ M OGB-1) and the calcium-insensitive fluorophore Alexa 594 (Invitrogen) via the whole-cell recording pipette and imaging the neuron with 2-photon microscopy (Fig. 1). In awake mice, CA1 pyramidal neurons often fire in high-frequency bursts of several APs at \sim 100 Hz (e.g., Ranck, 1973). We therefore evoked 1–4 APs at 100 Hz by somatic current injection and monitored the resulting calcium transients with line scans across the apical dendrite 50, 100, 125, 150, 175, and 200 μ m from the soma.

The resting fluorescence of OGB-1 was \sim 25% higher in neurons from 2-month-old Tg⁺ mice, relative to neurons from Tg⁻ littermates. OGB-1 fluorescence was elevated throughout the apical dendrite (Fig. 4D). Hence the resting intracellular calcium concentration was higher in the apical dendrites of neurons from Tg⁺ than Tg⁻ mice.

AP-evoked calcium transients measured in the proximal apical dendrite, 50 μ m from the soma, were not different in neurons from Tg⁺ and Tg⁻ mice (Fig. 4E). The calcium transients evoked by APs summed linearly during a burst of up to 4 APs (Fig. 4E), demonstrating that the indicator was

not nearing saturation in either Tg⁺ or Tg⁻ mice, even after 4APs.

In both Tg⁺ and Tg⁻ mice, the amplitudes of calcium signals evoked by a single AP declined with distance into the apical dendrite, as described previously (Spruston et al., 1995; Waters et al., 2005). This decline results from the decrease in AP amplitude during propagation into the apical dendrite, which causes the opening of fewer calcium channels in the distal than in the proximal dendrite (Spruston et al., 1995; Waters et al., 2005). The decline in amplitude of the calcium transient was greater in neurons from Tg⁺ than from Tg⁻ mice (Fig. 4G). For example, 175 μ m from the soma calcium signals evoked by 1, 2, 3, and 4 APs were all of smaller amplitude in Tg⁺ than in Tg⁻ mice (Fig. 4F). At this location, calcium signals in response to a single AP were detectable in Tg⁻, but not Tg⁺ mice. Hence AP-evoked dendritic calcium signals are impaired in CA1 pyramidal neurons from 2-month-old Tg⁺ mice. This is consistent with impaired propagation of the narrow AP into the apical dendrite in Tg⁺ mice and is likely to affect synaptic plasticity in these dendrites.

3.4. Cellular effects precede deficits in synaptic transmission

To determine whether these changes in the AP waveform and calcium metabolism precede or follow synaptic dysfunction in CRND8 mice, we characterized synaptic transmission onto CA1 pyramidal neurons. We examined three common measures of synaptic transmission: the paired-pulse ratio, the AMPA/NMDA ratio, and miniature EPSPs.

We delivered paired stimuli at frequencies of 5–40 Hz (interstimulus intervals of 25–200 ms; Fig. 5A). As expected, we observed paired-pulse facilitation which increased with paired-pulse frequency. The degree of facili-

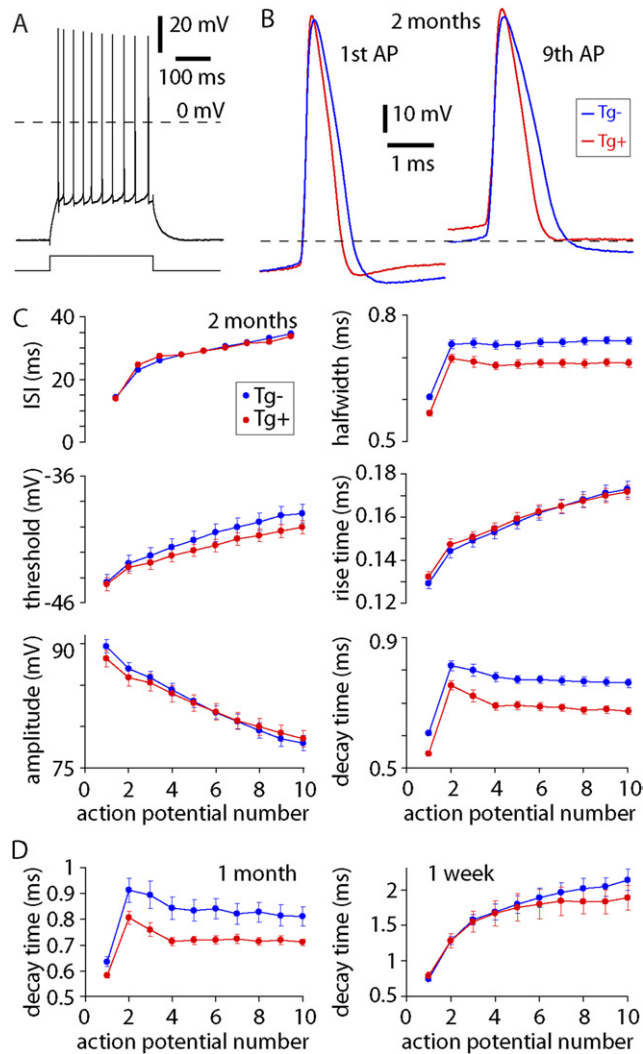


Fig. 3. Altered action potential (AP) waveforms in CA1 pyramidal neurons from young transgenic (Tg+) CRND8 mice. (A) Example of a train of 10 action potentials (APs) evoked by 300 ms current injection (200 pA) from a CA1 pyramidal neuron, 2-month-old mouse. (B) Examples of action potentials from trains of 10 APs, overlaid to allow comparison of AP waveforms of 2-month-old Tg+ (red) and Tg- (blue) mice. Dashed lines denote -40 mV. (C) Mean \pm standard error of the mean (SEM) interspike interval (ISI), AP threshold, AP amplitude, AP half width, 10%–90% rise time, and 10%–90% decay time during trains of 10 APs in 2-month-old Tg+ (red) and Tg- (blue) mice. $n = 54$ Tg- mice and 46 Tg+ mice. (D) 10%–90% decay times of APs during trains in CA1 pyramidal neurons from 1-month- and 1-week-old mice. $n = 14$ Tg- and 16 Tg+ mice at 1 month of age and 9 Tg- and 10 Tg+ mice at 1 week of age.

tation was no different in neurons from Tg+ and Tg- mice at 2, 4, or 6 months of age (Fig. 5B).

Next we measured the AMPA/NMDA ratio in 2 and 4-month-old mice. The AMPA/NMDA ratio is likely to change if A β has selective effects on synaptic AMPA or NMDA receptors, as has been suggested in other mouse models of APP overexpression and following application of A β oligomers (Snyder et al., 2005). We measured AMPA and NMDA receptor-mediated currents at -70 and $+40$

mV, respectively (Fig. 5C). The AMPA/NMDA ratio was similar in neurons from Tg+ and Tg- mice at 2 and 4 months of age.

Finally we monitored miniature EPSCs (mEPSCs) at -70 mV in $1 \mu\text{M}$ tetrodotoxin (Fig. 5F). There was no difference in the frequency or amplitude of mEPSCs in neurons from Tg+ and Tg- mice at 2, 3, or 4 months of age (Fig. 5F).

Hence we observed no differences in synaptic transmission in mice up to 4 months old and conclude that the changes in AP waveform and calcium metabolism in CA1 pyramidal neurons precede dysfunction of synaptic transmission in the Schaeffer collateral pathway in CRND8 mice.

3.5. Pharmacological relief of the difference in action potential waveform

In CA1 pyramidal neurons, the AP waveform is determined principally by sodium and potassium currents (Bean, 2007). It is likely, therefore, that the difference in AP waveform between Tg+ and Tg- mice results from a difference in one or more sodium or potassium currents. There are at least four potassium currents that can affect AP waveform in CA1 pyramidal neurons, principally by increasing its rate of decay (Bean, 2007): an A-type current (I_A ; Kim et al., 2005; Martina et al., 1998), a D-type current (I_D ; Golding et al., 1999; Grissmer et al., 1994; Martina et al., 1998; Wu and Barish, 1992), a 4-aminopyridine (4-AP)-sensitive fast delayed rectifier current ($I_{K,4-AP}$; Martina et al., 1998; Massengill et al., 1997), and a large-conductance calcium-activated current ($I_{K,Ca}$; Shao et al., 1999). During a train of APs, the relative levels of activation of these potassium currents change as a result of their different activation and inactivation characteristics. I_A and $I_{K,Ca}$ inactivate during a train of APs, resulting in progressive broadening of APs (Kim et al., 2005; Ma and Koester, 1995; Shao et al., 1999). Enhancing I_A or $I_{K,Ca}$ therefore results in a narrow, rapidly decaying AP and enhanced broadening and slowing of AP decay during a train. If I_A or $I_{K,Ca}$ were enhanced in Tg+ mice, this would therefore result in a convergence of AP half widths and decay times during trains in Tg+ and Tg- mice. In contrast I_D and $I_{K,4-AP}$ display increasing activation during a train of APs (Golding et al., 1999; Ma and Koester, 1995), resulting in a narrow, rapidly decaying AP and decreased broadening during a train. The difference between AP width and decay time in Tg+ and Tg- mice increases during trains of APs (Fig. 3), suggesting the likely involvement of I_D and/or $I_{K,4-AP}$.

To determine which of these currents might be altered in CRND8 mice, we compared AP waveforms in neurons from Tg+ and Tg- mice in the presence of blockers of these currents (Fig. 6). The difference in AP waveform between Tg+ and Tg- mice was eliminated by $300 \mu\text{M}$ tetraethylammonium ions (TEA), which block $I_{K,4-AP}$ and $I_{K,Ca}$. The

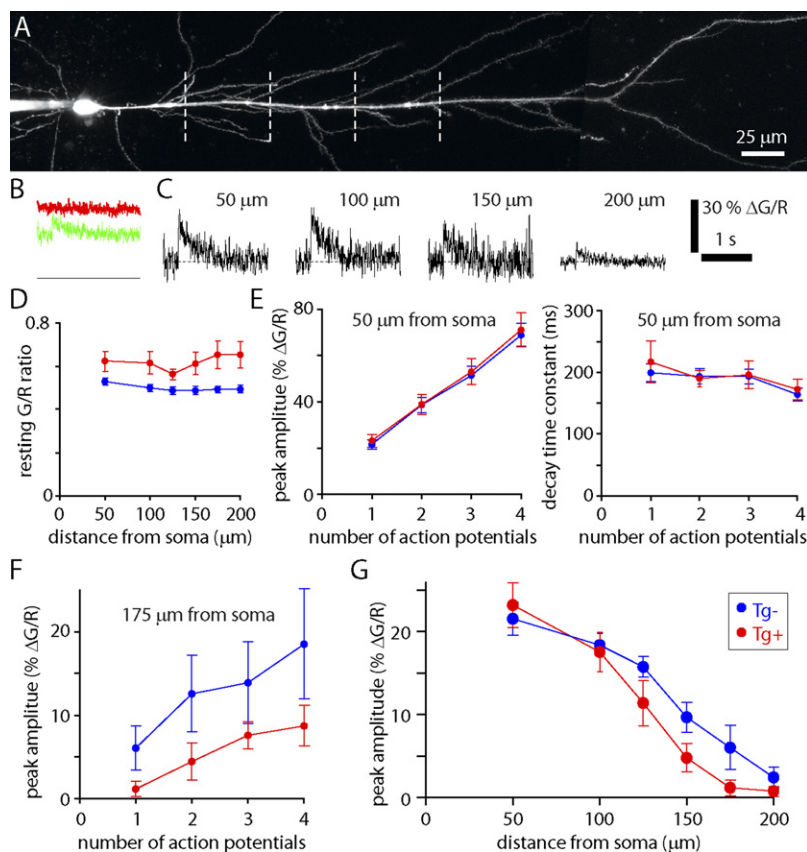


Fig. 4. Altered calcium metabolism in the apical dendrites of 2-month-old transgenic (Tg)⁺ mice. (A) Maximum intensity projection of the apical dendritic arbor of a CA1 pyramidal neuron filled with Oregon green BAPTA 488-1 (OGB-1) and Alexa 594 (Invitrogen, Carlsbad, CA, USA). Dashed line: locations at which calcium transients were measured (50, 100, 150, and 200 μm from the soma). The soma and somatic recording pipette are on the left of the image. (B) Example calcium transients evoked by a single action potential in the neuron in A. The left-most panel shows raw OGB-1 (green) and Alexa 594 (Invitrogen) (red) signals from a single trial, measured 50 μm from the soma. Fluorescence is shown on an arbitrary fluorescence scale, with a zero fluorescence baseline. (C) Examples of action potential (AP)-evoked fluorescence transients in the neuron in A. Transients were evoked by a single AP. Measurements 50, 100, and 150 μm from the soma are single trials. The 200-μm measurement is the average of 13 trials. (D) Mean ± standard error of the mean (SEM) resting G/R ratios from Tg⁺ and Tg⁻ mice, measured in the apical dendrite 50 to 200 μm from the soma. *n* = 9 Tg⁻ (blue) and 7 Tg⁺ (red) neurons. (E) Peak amplitudes and decay time constants for calcium transients evoked by 1–4 APs, measured 50 μm from the soma. *n* = 9 Tg⁻ and 7 Tg⁺ neurons. (F) Peak amplitudes of calcium transients evoked by 1–4 APs, measured 175 μm from the soma. *n* = 8 Tg⁻ and 6 Tg⁺ neurons. (G) Peak amplitudes of calcium transients evoked by single APs as a function of distance from the soma. *n* = 9 Tg⁻ and 7 Tg⁺ neurons.

difference was also eliminated by 100 μM 4-AP, which blocks $I_{K,4-AP}$ and I_D . Dendrotoxin (100 nM), which blocks I_D , failed to eliminate the difference in AP waveform. These results suggest that a fast delayed rectifier might be responsible for the difference in AP waveform between Tg⁺ and Tg⁻ mice.

3.6. Expression pattern of *Kv 3.1b* may be altered in 2-month-old CRND8 mice

A narrowing in AP waveform via an effect on a fast delayed rectifier might result from a change in the properties or from increased expression of the current. Hence we next examined levels of expression of several sodium and potassium currents that might be involved in shaping the AP waveform in CA1 pyramidal neurons. We performed immunohistochemistry using primary antibodies against the main genes expressed in CA1 pyramidal neurons (Supple-

mentary Table s3), corresponding to a slow delayed rectifier (I_K ; $Kv 1.1$ and $Kv 1.2$), $I_{K,4-AP}$ ($Kv 3.1b$), I_A ($Kv 4.2$, $Kv 4.3$), $I_{K,Ca}$ (SLO1), and two sodium currents ($Nav 1.1$ and $Nav 1.2$).

For all of these antibodies, staining patterns for both Tg⁺ and Tg⁻ mice were similar to published results (Fig 7A). Overall immunofluorescence intensities were also similar in sections from Tg⁺ and Tg⁻ mice for all 8 antibodies (Fig. 7B). However, there was a difference in the relative intensities of anti-*Kv 3.1b* immunofluorescence in stratum radiatum, oriens, and pyramidale. For each section, we calculated a “fluorescence distribution ratio” by dividing the immunofluorescence in stratum pyramidale by the mean fluorescence of stratum oriens and stratum radiatum. This ratio normalizes for any variation in staining between slices. We found that the fluorescence distribution ratio for *Kv 3.1b* was significantly greater in hippocampi from in Tg⁺ than

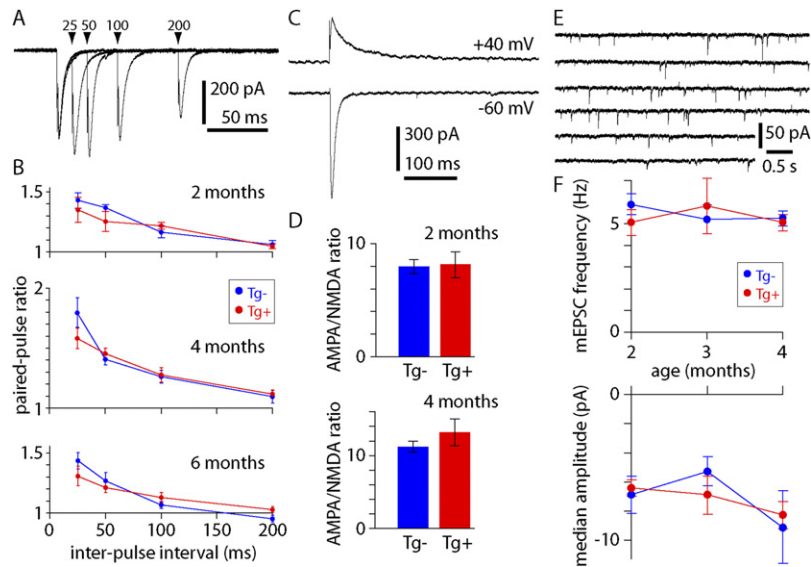


Fig. 5. Synaptic transmission in young transgenic (Tg⁺) and Tg⁻ mice. (A) Four overlaid traces showing excitatory postsynaptic currents (EPSCs) recorded from a 2-month-old Tg⁻ mouse. Paired-pulse protocol with interpulse intervals of 25, 50, 100, and 200 ms. (B) Paired-pulse ratios at 2, 4, and 6 months of age; 2 months $n = 6$ Tg⁻ and 5 Tg⁺ neurons; 4 months $n = 11$ Tg⁻ and 13 Tg⁺ neurons; 6 months $n = 8$ Tg⁻ and 8 Tg⁺ neurons. (C) Examples of EPSCs recorded from a 4-month-old Tg⁺ mouse at -60 and $+40$ mV, from which AMPA/NMDA ratios were calculated. (D) AMPA/NMDA ratios in Tg⁺ and Tg⁻ mice at 2 and 4 months of age. 2 months $n = 4$ Tg⁻ and 3 Tg⁺ neurons; 4 months $n = 5$ Tg⁻ and 6 Tg⁺ neurons. (E) Miniature EPSCs (mEPSCs) recorded from a 2-month-old Tg⁺ mouse. (F) mEPSC frequency and amplitude at 2, 3, and 4 months of age; 2 months $n = 10$ Tg⁻ and 10 Tg⁺ neurons; 3 months $n = 5$ Tg⁻ and 6 Tg⁺ neurons; 4 months $n = 7$ Tg⁻ and 10 Tg⁺ neurons.

Tg⁻ mice, while the distribution ratios were not different for any of the other 8 channels. These results suggest that there is a change in expression or accumulation of Kv 3.1b in Tg⁺ mice. This change is selective in that no such changes occur for the other channels examined. Hence our immunohistochemistry results are consistent with a narrowing of AP waveform as a result of increased expression or redistribution of a Kv3-type fast delayed rectifier potassium current in CA1 hippocampal pyramidal neurons in Tg⁺ CRND8 mice.

4. Discussion

We have identified two intrinsic cellular properties of CA1 hippocampal pyramidal neurons that differ between Tg⁺ CRND8 mice and Tg⁻ littermates: neurons from Tg⁺ mice have narrow action potentials, with a rapid decay, and an elevated resting intracellular calcium concentration. Both of these differences exist before plaque formation and before profound synaptic dysfunction. Of the many functional parameters studied, only these two differences were observed, suggesting that these two differences are probably the earliest functional changes in pyramidal neurons.

Accumulation of A β , following overexpression of human APP, is the principle distinction between Tg⁺ and Tg⁻ CRND8 mice. Hence it is likely that these differences in CA1 pyramidal neurons result from exposure to A β . Because these changes occur before plaque formation, the narrowing of the action potential and increase in resting

intracellular calcium are likely to be effects of soluble forms of A β .

4.1. Mechanism underlying narrow APs in CRND8 mice

Our pharmacology experiments suggest that changes in a fast delayed rectifier current underlie the narrow action potential in Tg⁺ CRND8 mice. However, these pharmacology experiments do not conclusively identify the fast delayed rectifier as the responsible current. Although nonselective at high concentrations, TEA and 4-AP are selective blockers of $I_{K,4-AP}$ and $I_{K,Ca}$ and of $I_{K,4-AP}$, I_A , and I_D , respectively, in CA1 pyramidal neurons at the concentrations employed here (Grissmer et al., 1994; Martina et al., 1998; Rettig et al., 1992). However, blocking one ion channel can affect the roles of other ion channels involved in repolarization after the AP (e.g., Ma and Koester, 1995, 1996). Hence it is possible that the effects of TEA and 4-AP involve another ion current that participates in repolarization of the AP.

Our immunohistochemistry experiments support the suggestion that expression of a fast delayed rectifier is altered in Tg⁺ CRND8 mice. First we found that the expression levels and patterns of many channels involved in repolarization of the AP are similar in Tg⁺ and Tg⁻ mice. Immunohistochemistry is probably only sensitive enough to detect substantial changes in expression of these channels, and we cannot therefore exclude some changes in other channels. However, we found that the pattern of expression

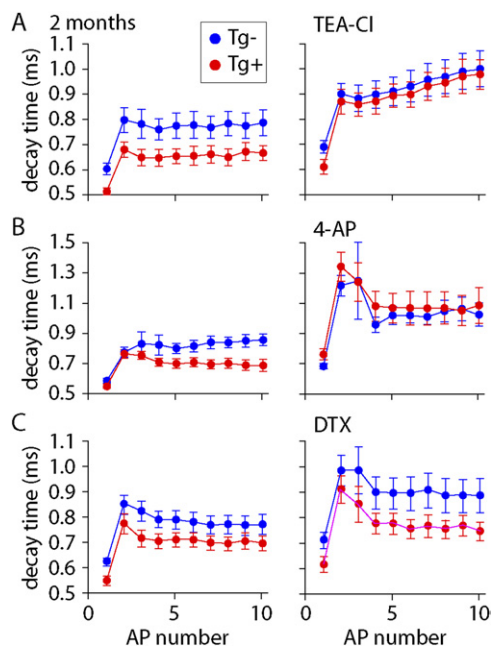


Fig. 6. Pharmacological pageade of difference in action potential (AP) waveform. (A–C) Effects of potassium channel blockers on the 90%–10% decay times of action potentials in 2-month-old CRND8 mice. Decay times are reported for trains for 10 APs. Each symbol is the mean \pm standard error of the mean (SEM) for Tg $^{-}$ (blue) or Tg $^{+}$ mice (red). In each recording decay times were measured first under control conditions (left) and the after application of blocker (right). (A) Effect of 300 μ M tetraethylammonium chloride (TEA-CI); $n = 5$ Tg $^{-}$ and 6 Tg $^{+}$ neurons. Decay times were significantly different under control conditions ($p < 0.05$) and this difference was eliminated by TEA ($p > 0.05$). (B) Effect of 100 μ M 4-aminopyridine (4-AP); $n = 7$ Tg $^{-}$ and 6 Tg $^{+}$ neurons. Decay times were significantly different under control conditions ($p < 0.05$) and this difference was eliminated by 4-AP ($p > 0.05$). (C) No effect of 100 nM dendrotoxin (DTX); $n = 10$ Tg $^{-}$ and 10 Tg $^{+}$ neurons. Decay times were significantly different under control conditions ($p < 0.05$) and in DTX ($p < 0.05$).

of only Kv3.1b was significantly altered in CRND8 mice. The Kv3 family is the principle family of fast delayed rectifier potassium channels expressed in hippocampus (Weiser et al., 1994). Kv3 channels are expressed in hippocampal pyramidal neurons, although the current density is lower than in interneurons, where Kv3-family currents contribute to rapid repolarization after the action potential (Martina et al., 1998; Weiser et al., 1994). Hence Kv3 expression was not limited to pyramidal neurons in our experiments and we were unable to determine whether the altered pattern of expression of Kv3.1b reflects expression by pyramidal neurons or other cells within the hippocampus.

Together, our pharmacology and immunohistochemistry results indicate that increased expression of Kv3 channels is the likely mechanism underlying the narrow AP in CA1 hippocampal pyramidal neurons in Tg $^{+}$ CRND8 mice.

4.2. Effects of A β on ion channels

There are many reports of effects of A β on plasma membrane potassium channels. For example, A β can en-

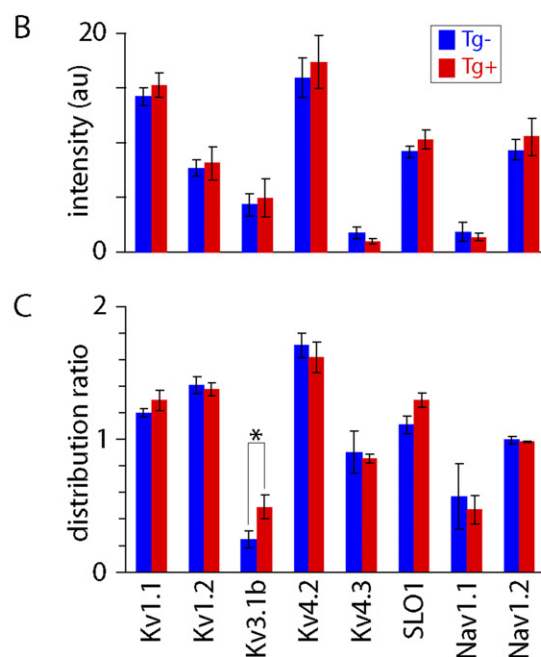
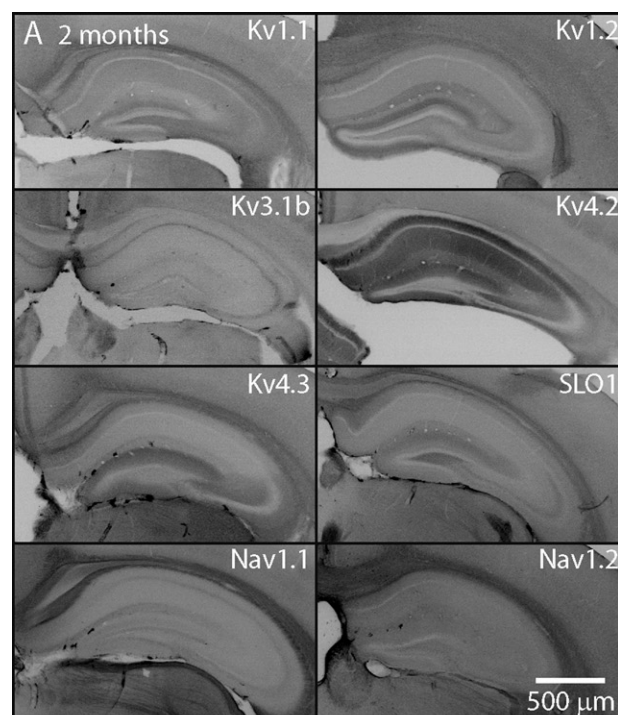


Fig. 7. Channel immunohistochemistry in 2-month-old CRND8 mice. (A) Widefield images of hippocampi from 2-month-old transgenic (Tg $^{+}$) mice stained for several potassium and sodium channels. Intensities were inverted for display purposes. (B) Fluorescence intensities in CA1 (arbitrary intensity units). Intensities were averaged across stratum oriens, stratum pyramidale and stratum radiatum. There was no significant difference in intensity between 2-month-old Tg $^{+}$ and Tg $^{-}$ mice immunostained with any of the antibodies tested. Each bar is the mean \pm standard error of the mean (SEM) of 3–7 mice, with 3–6 sections from each mouse. (C) Immuofluorescence intensities in stratum oriens and radiatum normalized to the intensity in stratum pyramidale in CA1. Fluorescence intensity differed between 2-month-old Tg $^{+}$ and Tg $^{-}$ mice only for Kv3.1b (asterisk denotes $p < 0.05$, unpaired t test).

hance I_A (Kerrigan et al., 2008; Plant et al., 2006), suppress I_A (Chen, 2005; Good et al., 1996), enhance $I_{K,Ca}$ (Ye et al., 2010), suppress $I_{K,Ca}$ (Coles et al., 2008; Qi and Qiao, 2001), and enhance Kv3.4 currents (Angulo et al., 2004; Pannaccione et al., 2007). How these effects depend on the species and concentration of A β and the duration of exposure to A β are unclear, making it difficult to assess which ion channels are most sensitive to the various forms of A β and how these changes might relate to the different stages of AD. Here we have described changes in potassium channels in the hippocampus of an established mouse model of APP overexpression. Our results suggest that, in CA1 hippocampal pyramidal neurons, the Kv3 family of ion channels are the first to be affected by prolonged exposure to a mixture of A β species, as occurs in AD.

4.3. Effects of A β on calcium metabolism

The second difference we observed between Tg+ and Tg- CRND8 mice is elevated resting calcium in Tg+ mice. A β has long been associated with dysfunctional calcium metabolism (Bezprozvanny and Mattson, 2008; Camandola and Mattson, 2011; Green and LaFerla, 2008). Application of A β can elevate intracellular calcium concentration in neurons (Mattson et al., 1992) and resting intracellular calcium may be elevated close to plaques in APP overexpressing mice (Kuchibhotla et al., 2008). Presenilin mutations have also been linked with dysregulation of calcium homeostasis (Stutzmann, 2005).

CRND8 mice do not carry a presenilin mutation. Hence the elevation in resting intracellular calcium in CA1 pyramidal neurons in CRND8 mice, observed here, probably results from A β overexpression. Furthermore, in our experiments resting calcium was elevated in young mice, before plaque formation, implicating soluble A β species in calcium dysregulation.

The signaling pathways underlying A β -mediated calcium dysfunction are poorly understood but are thought to involve oxidative stress pathways (Camandola and Mattson, 2011) or aberrant ryanodine receptor function (Supnet et al., 2006). A β oligomers can also affect intracellular calcium concentrations by forming calcium-permeable pores in the plasma membrane (Zhu et al., 2000) and by modulating influx through L-type calcium channels (Ekinci et al., 1999; Ueda et al., 1997). Ryanodine receptor function is known to be impaired in CRND8 mice (Supnet et al., 2006), but more research will be required to determine whether other mechanisms are also involved in elevating the resting intracellular calcium concentration in CRND8 mice.

Are the narrow AP and elevated resting calcium linked? We have demonstrated that one of the consequences of the narrow AP is a reduction in dendritic calcium influx during spiking. It is therefore tempting to speculate that the narrow AP is a homeostatic mechanism to reduce the calcium load, which occurs in response to the elevated resting calcium concentration.

4.4. Physiological and pathological consequences of the narrow AP

Whether or not the narrow AP is a compensatory mechanism, it is likely to have unfortunate consequences for the hippocampal network. First, a narrow AP might be prone to fail at branch points in the axonal tree (Goldstein and Rall, 1974) and when propagation occurs, a narrow AP may evoke relatively little calcium influx and transmitter release at presynaptic terminals. In CRND8 mice, the narrow AP might weaken signaling from CA1 pyramidal cells to their target neurons.

The narrow AP is also likely to affect dendritic function in CA1 pyramidal neurons. APs propagating into the apical dendritic tree, and the resulting calcium influx, play an important role in the induction of long-term synaptic plasticity, both long-term depression and long-term potentiation (Sjöström and Nelson, 2002; Waters et al., 2008). The suppression of AP-evoked dendritic calcium influx, as shown here, may contribute to the changes in long-term potentiation and depression in CA1 pyramidal neurons, described in CRND8 mice and many other APP-overexpressing mouse lines (Brown et al., 2005; Chapman et al., 1999; Dewachter et al., 2007; Jacobsen et al., 2006; Jolas et al., 2002; Knobloch et al., 2007). Long-term potentiation and depression are thought to be cellular substrates of learning and memory and the hippocampus is intimately associated with learning and memory and one of the early sites of degeneration in AD. The narrow AP in CA1 pyramidal neurons and resulting dysfunctional synaptic plasticity in hippocampus may therefore contribute to the learning and memory deficits observed in APP-overexpressing mice and in AD patients.

Here we have described changes in the intrinsic physiology of CA1 hippocampal pyramidal neurons in CRND8 mice. The changes we have described occur before plaque formation and before overt changes in synaptic function. Changes in synaptic function and the intrinsic properties of neurons will both influence information flow through the hippocampal network and our results therefore indicate that the effects of A β on CA1 pyramidal neurons are likely to combine with the well-known effects of A β on synaptic transmission to disrupt hippocampal network function. Indeed, because cellular changes precede synaptic dysfunction, the cellular effects may well be the primary basis of the earliest effects of A β on hippocampal networks.

Disclosure statement

There are no actual or potential conflicts of interest.

All experiments and procedures were approved by the Northwestern University Institutional Animal Care and Use Committee (IACUC).

Acknowledgements

The project was supported by NIRG-06-25509 from the Alzheimer's Association and 5R21AG029282-02 from the National Institute on Aging.

We thank Becky Imhoff for technical assistance and Pavel Osten, Bob Vassar, Marco Martina, Murali Prakriya, and Anis Contractor for discussions.

Appendix. Supplementary data

Supplementary data associated with this article can be found, in the online version, at doi:10.1016/j.neurobiolaging.2011.05.001.

References

- Ambrée, O., Touma, C., Görtz, N., Keyvani, K., Paulus, W., Palme, R., Sachser, N., 2006. Activity changes and marked stereotypic behavior precede Aβ pathology in TgCRND8 Alzheimer mice. *Neurobiol. Aging* 27, 955–964.
- Angulo, E., Noé, V., Casadó, V., Mallol, J., Gomez-Isla, T., Lluís, C., Ferrer, I., Ciudad, C.J., Franco, R., 2004. Up-regulation of the Kv3.4 potassium channel subunit in early stages of Alzheimer's disease. *J. Neurochem.* 10, 547–557.
- Bean, B.P., 2007. The action potential in mammalian central neurons. *Nat. Rev. Neurosci.* 8, 451–465.
- Bezprozvanny, I., Mattson, M.P., 2008. Neuronal calcium mishandling and the pathogenesis of Alzheimer's disease. *Trends Neurosci.* 31, 454–463.
- Brown, J.T., Richardson, J.C., Collingridge, G.L., Randall, A.D., Davies, C.H., 2005. Synaptic transmission and synchronous activity is disrupted in hippocampal slices taken from aged TAS10 mice. *Hippocampus* 15, 110–117.
- Camandola, S., Mattson, M.P., 2011. Aberrant subcellular neuronal calcium regulation in aging and Alzheimer's disease. *Biochim. Biophys. Acta* 1813, 965–973.
- Chauhan, N.B., Siegel, G.J., Lichter, T., 2004. Effect of age on the duration and extent of amyloid plaque reduction and microglial activation after injection of anti-Aβ antibody into the third ventricle of TgCRND8 mice. *J. Neurosci. Res.* 78, 732–741.
- Chapman, P.F., White, G.L., Jones, M.W., Cooper-Blacketer, D., Marshall, V.J., Irizarry, M., Younkin, L., Good, M.A., Bliss, T.V., Hyman, B.T., Younkin, S.G., Hsiao, K.K., 1999. Impaired synaptic plasticity and learning in aged amyloid precursor protein transgenic mice. *Nat. Neurosci.* 3, 271–276.
- Chen, C., 2005. β-Amyloid increases dendritic Ca²⁺ influx by inhibiting the A-type K⁺ current in hippocampal CA1 pyramidal neurons. *Biochem. Biophys. Res. Commun.* 338, 1913–1919.
- Chishti, M.A., Yang, D.-S., Janus, C., Phinney, A.L., Horne, P., Pearson, J., Strome, R., Zuker, N., Loukides, J., French, J., Turner, S., Lozza, G., Grilli, M., Kunicki, S., Morissette, C., Paquette, J., Gervais, F., Bergeron, C., Fraser, P.E., Carlson, G.A., St George-Hyslop, P., Westaway, D., 2001. Early-onset amyloid deposition and cognitive deficits in transgenic mice expressing a double mutant form of amyloid precursor protein 695. *J. Biol. Chem.* 276, 21562–21570.
- Clements, J.D., Bekkers, J.M., 1997. Detection of spontaneous synaptic events with an optimally scaled template. *Biophys. J.* 73, 220–229.
- Coles, B., Wilton, L.A., Good, M., Chapman, P.F., Wann, K.T., 2008. Potassium channels in hippocampal neurones are absent in a transgenic but not in a chemical model of Alzheimer's disease. *Brain Res.* 1190, 1–14.
- Dewachter, I., Filipkowski, R.K., Priller, C., Ris, L., Neyton, J., Croes, S., Terwel, D., Gysemans, M., Devijver, H., Borghgraef, P., Godaux, E., Kaczmarek, L., Herms, J., Van Leuven, F., 2007. Deregulation of NMDA-receptor function and down-stream signaling in APP[V717I] transgenic mice. *Neurobiol. Aging* 2, 241–256.
- Ekinci, F.J., Malik, K.U., Shea, T.B., 1999. Activation of the L voltage-sensitive calcium channel by mitogen-activated protein (MAP) kinase following exposure of neuronal cells to beta-amyloid. MAP kinase mediates beta-amyloid-induced neurodegeneration. *J. Biol. Chem.* 274, 30322–30327.
- Golding, N.L., Jung, H.Y., Mickus, T., Spruston, N., 1999. Dendritic calcium spike initiation and repolarization are controlled by distinct potassium channel subtypes in CA1 pyramidal neurons. *J. Neurosci.* 19, 8789–8798.
- Goldstein, S.S., Rall, W., 1974. Changes of action potential shape and velocity for changing core conductor geometry. *Biophys. J.* 14, 731–757.
- Good, T.A., Smith, D.O., Murphy, R.M., 1996. β-amyloid peptide blocks the fast-inactivating k⁺ current in rat hippocampal neurons. *Biophys. J.* 70, 296–304.
- Green, K.N., LaFerla, F.M., 2008. Linking calcium to Aβ and Alzheimer's Disease. *Neuron* 59, 190–194.
- Grissmer, S., Nguyen, A.N., Aiyar, J., Hanson, D.C., Mather, R.J., Guttman, G.A., Karmilowicz, M.J., Auperin, D.D., Chandy, K.G., 1994. Pharmacological characterization of five cloned voltage-gated K⁺ channels, types Kv1.1, 1.2, 1.3, 1.5, and 3.1, stably expressed in mammalian cell lines. *Mol. Pharmacol.* 45, 1227–1234.
- Guntern, R., Bouras, C., Hof, P.R., Vallet, P.G., 1992. An improved thioflavine S method for staining neurofibrillary tangles and senile plaques in Alzheimer's disease. *Experientia* 48, 8–10.
- Hardy, J., 2006. A hundred years of Alzheimer's disease research. *Neuron* 52, 3–13.
- Hardy, J., Selkoe, D.J., 2002. The amyloid hypothesis of Alzheimer's disease: progress and problems on the road to therapeutics. *Science* 297, 353–356.
- Hsia, A.Y., Masliah, E., McConlogue, L., Yu, G.Q., Tatsuno, G., Hu, K., Kholodenko, D., Malenka, R.C., Nicoll, R.A., Mucke, L., 1999. Plaque-independent disruption of neural circuits in Alzheimer's disease mouse models. *Proc. Natl. Acad. Sci. U. S. A.* 96, 3228–3233.
- Hyde, L.A., Kazdoba, T.M., Grilli, M., Lozza, G., Brusa, R., Zhang, Q., Wong, G.T., McCool, M.F., Zhang, L., Parker, E.M., Higgins, G.A., 2005. Age-progressing cognitive impairments and neuropathology in transgenic CRND8 mice. *Behav. Brain Res.* 160, 344–355.
- Jacobsen, J.S., Wu, C.C., Redwine, J.M., Comery, T.A., Arias, R., Bowlby, M., Martone, R., Morrison, J.H., Pangalos, M.N., Reinhart, P.H., Bloom, F.E., 2006. Early-onset behavioral and synaptic deficits in a mouse model of Alzheimer's disease. *Proc. Natl. Acad. Sci. U. S. A.* 103, 5161–5166.
- Jolas, T., Zhang, X.S., Zhang, Q., Wong, G., Del Vecchio, R., Gold, L., Priestley, T., 2002. Long-term potentiation is increased in the CA1 area of the hippocampus of APP(swe/ind) CRND8 mice. *Neurobiol. Dis.* 11, 394–409.
- Kerrigan, T.L., Atkinson, L., Peers, C., Pearson, H.A., 2008. Modulation of 'A'-type K⁺ current by rodent and human forms of amyloid β protein. *Neuroreport* 19, 839–843.
- Kim, J., Wei, D.-S., Hoffman, D.A., 2005. Kv4 potassium channel subunits control action potential repolarization and frequency-dependent broadening in rat hippocampal CA1 pyramidal neurons. *J. Physiol.* 569, 41–57.
- Kim, J.H., Anwyl, R., Suh, Y.H., Djamgoz, M.B., Rowan, M.J., 2001. Use-dependent effects of amyloidogenic fragments of (beta)-amyloid precursor protein on synaptic plasticity in rat hippocampus in vivo. *J. Neurosci.* 21, 1327–1333.
- Kim, K.S., Miller, D.L., Sapienza, V.J., Chen, C.-M.J., Bai, C., Grundke-Iqbal, I., Currie, J.R., Wisniewski, H.M., 1988. Production and characterization of monoclonal antibodies reactive to synthetic cerebrovascular amyloid peptide. *Neurosci Res Comm* 2, 121–130.

- Kim, K.S., Wen, G.Y., Bancher, C., Chen, C.M.J., Sapienza, V.J., Hong, H., Wisniewski, H.M., 1990. Detection and quantitation of amyloid β -peptide with 2 monoclonal antibodies. *Neurosci Res Comm* 7, 113–122.
- Knobloch, M., Farinelli, M., Konietzko, U., Nitsch, R.M., Mansuy, I.M., 2007. Abeta oligomer-mediated long-term potentiation impairment involves protein phosphatase 1-dependent mechanisms. *J. Neurosci.* 27, 7648–7653.
- Kuchibhotla, K.V., Goldman, S.T., Lattarulo, C.R., Wu, H.Y., Hyman, B.T., Bacskaï, B.J., 2008. A β plaques lead to aberrant regulation of calcium homeostasis in vivo resulting in structural and functional disruption of neuronal networks. *Neuron* 59, 214–225.
- Larson, J., Lynch, G., Games, D., Seubert, P., 1999. Alterations in synaptic transmission and long-term potentiation in hippocampal slices from young and aged PDAPP mice. *Brain Res.* 840, 23–35.
- LeVine, H., 1999. Quantification of β -sheet amyloid fibril structures with thioflavin T. *Meth. Enzymol.* 309, 274–284.
- Li, S., Hong, S., Shepardson, N.E., Walsh, D.M., Shankar, G.M., Selkoe, D., 2009. Soluble oligomers of amyloid β protein facilitate hippocampal long-term depression by disrupting neuronal glutamate uptake. *Neuron* 62, 788–801.
- Ma, M., Koester, J., 1995. Consequences and mechanisms of spike broadening of R20 cells in *Aplysia californica*. *J. Neurosci.* 15, 6720–6734.
- Ma, M., Koester, J., 1996. The role of K⁺ currents in frequency-dependent spike broadening in *Aplysia* R20 neurons: a dynamic-clamp analysis. *J. Neurosci.* 16, 4089–4101.
- Martina, M., Schultz, J.H., Ehmke, H., Monyer, H., Jonas, P., 1998. Functional and molecular differences between voltage-gated K⁺ channels of fast-spiking interneurons and pyramidal neurons of rat hippocampus. *J. Neurosci.* 18, 8111–8125.
- Massengill, J.L., Smith, M.A., Son, D.I., O'Dowd, D.K., 1997. Differential expression of K_{4-AP} currents and Kv3.1 potassium channel transcripts in cortical neurons that develop distinct firing phenotypes. *J. Neurosci.* 17, 3136–3147.
- Masters, C.L., Simms, G., Weinman, N.A., Multhaup, G., McDonald, B.L., Beyreuther, K., 1985. Amyloid plaque core protein in Alzheimer disease and Down syndrome. *PNAS.* 82, 4245–4249.
- Mattson, M.P., Cheng, B., Davis, D., Bryant, K., Lieberburg, I., Rydel, R.E., 1992. beta-Amyloid peptides destabilize calcium homeostasis and render human cortical neurons vulnerable to excitotoxicity. *J. Neurosci.* 12, 376–389.
- Nomura, I., Kato, N., Kita, T., Takechi, H., 2005. Mechanism of impairment of long-term potentiation by amyloid beta is independent of NMDA receptors or voltage-dependent calcium channels in hippocampal CA1 pyramidal neurons. *Neurosci. Lett.* 391, 1–6.
- Oertner, T.G., Sabatini, B.L., Nimchinsky, E.A., Svoboda, K., 2002. Facilitation at single synapses probed with optical quantal analysis. *Nat. Neurosci.* 5, 657–664.
- Palop, J.J., Mucke, L., 2010. Amyloid- β -induced neuronal dysfunction in Alzheimer's disease: from synapses toward neural networks. *Nat. Neurosci.* 13, 812–818.
- Pannaccione, A., Boscia, F., Scorziello, A., Adornetto, A., Castaldo, P., Sirabella, R., Tagliatela, M., Di Renzo, G.F., Annunziato, L., 2007. Up-regulation and increased activity of Kv3.4 channels and their accessory subunit MinK-related peptide 2 induced by amyloid peptide are involved in apoptotic neuronal death. *Mol. Pharm.* 72, 665–673.
- Plant, L.D., Webster, N.J., Boyle, J.P., Ramsden, M., Freir, D.B., Peers, C., Pearson, H.A., 2006. Amyloid β peptide as a physiological modulator of neuronal "A"-type K⁺ current. *Neurobiol. Aging* 27, 1673–1683.
- Qi, J.S., Qiao, J.T., 2001. Suppression of large conductance Ca²⁺-activated K⁺ channels by amyloid β -protein fragment 31–35 in membrane patches excised from hippocampal neurons. *Acta Physiol. Sin.* 53, 198–204.
- Ranck, J.B., 1973. Studies on single neurons in dorsal hippocampal formation and septum in unrestrained rats. I. Behavioral correlates and firing repertoires. *Exp. Neurol.* 41, 461–531.
- Raymond, C.R., Ireland, D.R., Abraham, W.C., 2003. NMDA receptor regulation by amyloid-beta does not account for its inhibition of LTP in rat hippocampus. *Brain Res.* 968, 263–272.
- Rettig, J., Wunder, F., Stocker, M., Lichtiginghagen, R., Mastiaux, F., Beckh, S., Kues, W., Pedarzani, P., Schröter, K.H., Ruppersberg, J.P., Veh, R., Pongs, O., 1992. Characterization of a *Shaw*-related potassium channel family in rat brain. *EMBO J.* 11, 2473–2486.
- Sabatini, B.L., Oertner, T.G., Svoboda, K., 2002. The life cycle of Ca(2+) ions in dendritic spines. *Neuron* 33, 439–452.
- Shankar, G.M., Li, S., Mehta, T.H., Garcia-Munoz, A., Shepardson, N.E., Smith, I., Brett, F.M., Farrell, M.A., Rowan, M.J., Lemere, C.A., Regan, C.M., Walsh, D.M., Sabatini, B.L., Selkoe, D.J., 2008. Amyloid-beta protein dimers isolated directly from Alzheimer. *Nat. Med.* 14, 837–842.
- Shao, L.-R., Halvorsrud, R., Borg-Graham, L., Storm, J.F., 1999. The role of BK-type Ca²⁺-dependent K⁺ channels in spike broadening during repetitive firing in rat hippocampal pyramidal cells. *J. Physiol.* 521, 135–146.
- Sjöström, P.J., Nelson, S.B., 2002. Spike timing, calcium signals and synaptic plasticity. *Curr. Opin. Neurobiol.* 12, 305–314.
- Small, D.H., Mok, S.S., Bornstein, J.C., 2001. Alzheimer's disease and Abeta toxicity: From top to bottom. *Nat. Rev. Neurosci.* 2, 595–598.
- Snyder, E.M., Nong, Y., Almeida, C.G., Paul, S., Moran, T., Choi, E.Y., Nairn, A.C., Salter, M.W., Lombroso, P.J., Gouras, G.K., Greengard, P., 2005. Regulation of NMDA receptor trafficking by amyloid- β . *Nat. Neurosci.* 8, 1051–1058.
- Spruston, N., Schiller, Y., Stuart, G., Sakmann, B., 1995. Activity-dependent action potential invasion and calcium influx into hippocampal CA1 dendrites. *Science* 268, 297–300.
- Stutzmann, G.E., 2005. Calcium dysregulation, IP3 signaling, and Alzheimer's Disease. *Neuroscientist* 11, 110–115.
- Supnet, C., Grant, J., Kong, H., Westaway, D., Mayne, M., 2006. Amyloid-beta-(1-42) increases ryanodine receptor-3 expression and function in neurons of TgCRND8 mice. *J. Biol. Chem.* 281, 38440–38447.
- Townsend, M., Shankar, G.M., Mehta, T., Walsh, D.M., Selkoe, D.J., 2006. Effects of secreted oligomers of amyloid β -protein on hippocampal synaptic plasticity: a potent role for trimers. *J. Physiol.* 572, 477–492.
- Ueda, K., Shinohara, S., Yagami, T., Asakura, K., Kawasaki, K., 1997. Amyloid β protein potentiates Ca²⁺ influx through L-type voltage-sensitive Ca²⁺ channels: a possible involvement of free radicals. *J. Neurochem.* 68, 265–271.
- Walsh, D.M., Klyubin, I., Fadeeva, J.V., Cullen, W.K., Anwyl, R., Wolfe, M.S., Rowan, M.J., Selkoe, D.J., 2002. Naturally secreted oligomers of amyloid beta protein potently inhibit hippocampal long-term potentiation in vivo. *Nature* 416, 535–539.
- Wang, H.W., Pasternak, J.F., Kuo, H., Ristic, H., Lambert, M.P., Chromy, B., Viola, K.L., Klein, W.L., Stine, W.B., Krafft, G.A., Trommer, B.L., 2002. Soluble oligomers of β amyloid (1–42) inhibit long-term potentiation but not long-term depression in rat dentate gyrus. *Brain Res.* 924, 133–140.
- Wang, Q., Walsh, D.M., Rowan, M.J., Selkoe, D.J., Anwyl, R., 2004. Block of long-term potentiation by naturally secreted and synthetic amyloid beta-peptide in hippocampal slices is mediated via activation of the kinases c-Jun N-terminal kinase, cyclin-dependent kinase 5, and p38 mitogen-activated protein kinase as well as metabotropic glutamate receptor type 5. *J. Neurosci.* 24, 3370–3378.
- Waters, J., Helmchen, F., 2006. Background synaptic activity is sparse in neocortex. *J. Neurosci.* 26, 8267–8277.
- Waters, J., Nevian, T., Sakmann, B., Helmchen, F., 2008. Action potentials in dendrites and spike-timing-dependent plasticity, in: Sweatt, J.D. (Ed.), *Molecular Mechanisms of Memory*. Vol. 4 of *Learning and Memory*. A Comprehensive Reference, Elsevier, Oxford, pp. 803–828.
- Zhu, Y.J., Lin, H., Lal, R., 2000. Fresh and nonfibrillar amyloid β protein(1–40) induces rapid cellular degeneration in aged human fibroblasts: evidence for A β -channel-mediated cellular toxicity. *FASEB J.* 14, 1244–1254.

- Waters, J., Schaefer, A., Sakmann, B., 2005. Backpropagating action potentials in neurones: measurement, mechanisms and potential functions. *Prog. Biophys. Mol. Biol.* 87, 145–170.
- Weiser, M., Vega-Saenz de Miera, E., Kentros, C., Moreno, H., Franzen, L., Hillman, D., Baker, H., Rudy, B., 1994. Differential expression of Shaw-related K⁺ channels in the rat central nervous system. *J. Neurosci.* 14, 949–972.
- Wu, R.L., Barish, M.E., 1992. Two pharmacologically and kinetically distinct transient potassium currents in cultured embryonic mouse hippocampal neurons. *J. Neurosci.* 12, 2235–2246.
- Ye, H., Jalini, S., Mylvaganam, S., Carlen, P., 2010. Activation of large-conductance Ca(2+)-activated K(+) channels depresses basal synaptic transmission in the hippocampal CA1 area in APP (swe/ind) TgCRND8 mice. *Neurobiol. Aging* 31, 591–604.